

# Stranded Wire With Uninsulated Strands as a Low-Cost Alternative to Litz Wire

Xu Tang  
C. R. Sullivan

Found in *IEEE Power Electronics Specialists Conference*, June 2003,  
pp. 289–295.

©2003 IEEE. Personal use of this material is permitted. However, permission to reprint or republish this material for advertising or promotional purposes or for creating new collective works for resale or redistribution to servers or lists, or to reuse any copyrighted component of this work in other works must be obtained from the IEEE.

# Stranded Wire With Uninsulated Strands as a Low-Cost Alternative to Litz Wire

Xu Tang and Charles R. Sullivan

xu.tang@dartmouth.edu

charles.r.sullivan@dartmouth.edu

<http://engineering.dartmouth.edu/inductor>

8000 Cummings Hall, Dartmouth College, Hanover, NH 03755, USA

Tel. +1-603-646-2851 Fax +1-603-646-3856

**Abstract**—High-frequency loss in transformer windings using stranded wire is analyzed. A complete loss prediction method is presented. The interstrand resistivity, which is an important parameter to determine the power loss, is measured experimentally. The analytical model is solved to get an optimal pitch, which specifies the degree of twisting that results in minimum loss. A transformer using a stranded wire winding is built and measured. The model prediction is verified to have high accuracy in the frequency range up to 100 kHz. Compared with the same transformer using a solid wire winding, about 67 percent less power loss at 100 kHz is achieved using stranded wire. Using the loss-prediction model provided in this paper, engineers will be able to control eddy-current losses in high-frequency transformer and inductor windings using stranded wire at a relatively low cost compared to using litz wire.

## I. INTRODUCTION

Special winding construction, using litz wire or foil, is often necessary to control eddy-current losses in high-frequency transformer and inductor windings. The high cost of these techniques is a major limitation in developing high-power-density, high-efficiency components for power electronics. A much lower-cost alternative is simple stranded copper wire with uninsulated, bare strands. In addition to the wire cost advantage arising from avoiding the insulation process, there is a component-manufacturing cost advantage arising from the easier termination of bare strands. The loss with uninsulated strands will certainly be higher than in true litz wire with individually insulated strands. However, the high-frequency loss can be substantially lower than in solid wire—the separation into strands impedes eddy currents, even if it does not completely stop them. Anecdotal evidence has supported the idea that this can work well in some applications. However, until now, there has not been a model available to predict the eddy-current losses in stranded wire with uninsulated strands, which we will refer to simply as *stranded wire* for the remainder of this paper. Thus, it has not been possible for a designer to evaluate this low-cost alternative and determine whether it is a good choice for a particular application, and it is almost never used.

In this paper, we develop a model to predict losses in stranded wire, by combining standard analysis of loss in litz wire [1], [2], [3], [4] with new analysis of the currents that circulate between uninsulated strands. An important parameter in this model, the resistance between strands, needed to be determined experimentally; these measurements are described in Section III. The model has been verified experimentally as described in Section V. The discrepancy between the prediction and the measurement at very high frequency was explained in

This work was supported in part by the United States Department of Energy under grant DE-FC36-01GO1106.

Section V-A. The experiments also confirm performance much better than that of solid wire.

With a verified model for the losses in stranded wire, it is possible to quantitatively evaluate its performance in a particular application. In some cases, its performance can be very similar to that of true litz wire, whereas in other situations, its losses are substantially higher. Thus, our model provides an important tool to designers, allowing them to take advantage of the cost savings of uninsulated strands where they work well, while avoiding them where they do not.

Because we provide an analytical model of loss, it is possible to use it in analytical design optimization. In Section IV, we present the optimization of one important parameter: the degree of twisting in a bundle, as quantified by pitch, the distance for one full twist. Tight twisting (shorter pitch) results in smaller loops linking ac flux, and thus lower circulating currents and ac loss. However, short pitch also results in longer length of each strand, due to the twisted path it must follow, and this leads to an increase in other types of eddy-current loss and to larger dc resistance. Our optimization provides the pitch giving minimum total loss in stranded wire.

## II. LOSS CALCULATION

Skin effect and proximity effect are the two effects that make the current density distributions non-uniform at high frequency, and thus increase the power loss. Skin effect is the tendency for high-frequency currents to flow on the surface of a conductor. Proximity effect is the tendency for current to flow in other undesirable patterns—loops or concentrated distributions—due to the presence of magnetic fields generated by nearby conductors. Ordinarily, proximity effects dominate skin effects in a transformer or inductor because in a multi-layer winding the total magnetic field is much larger than the field generated only by one strand or turn.

In multi-strand windings, skin and proximity effects may be further divided into strand-level and bundle-level effects, as illustrated in Fig. 1. Bundle-level effects relate to current circulating in paths involving multiple strands, whereas strand-level effects take place within individual strands. Strand-level proximity effect may optionally be still further divided into internal proximity effect (the effect of other currents within the bundle) and external proximity effect, but we instead consider the total proximity effect as a result of the total field at any given strand.

Strand-level effects are not significantly affected by the presence or absence of insulation except as discussed in Section V-A. Thus, standard litz-wire analysis [1], [2], [3], [4] can be applied to uninsulated strands. Predicting bundle-level

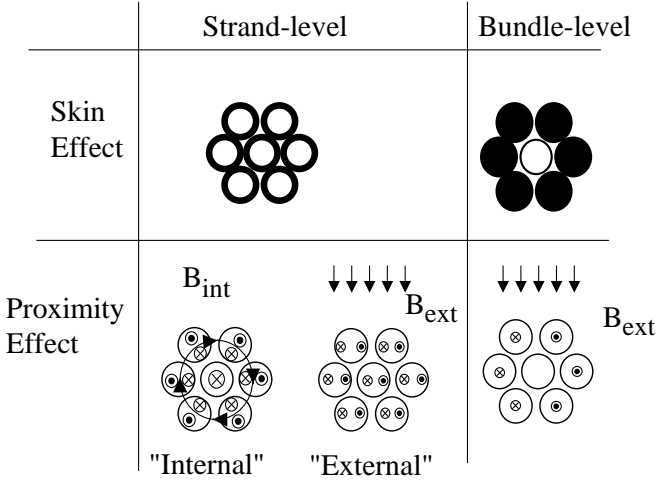


Fig. 1. Types of eddy-current effects in bundled wire.

proximity effect with finite conductivity between strands is more complex. The potential between any pair of strands induced by changing magnetic field is calculated, and then the current and loss are determined based upon the measured resistance between strands.

Because we find that the bundle-level proximity effect losses are reduced by using smaller pitch, it is important to include the effect of pitch on dc resistance and on strand-level proximity effect in our analysis. The calculations of each type of loss, including pitch effects, are outlined below.

#### A. DC resistance

The distance a strand travels is longer when it is twisted than when it goes straight. The effect of twisting on the length of strand is illustrated in Fig. 2, which shows a single cylindrical shell of length equal to the pitch, unwound to show flat on the page. With simple twisting, each strand will stay within one such shell at a radius  $r$ , and thus will be longer than the overall bundle by a factor of

$$\frac{\ell_d}{p} = \frac{1}{\cos(\theta)} = \frac{\sqrt{p^2 + (2\pi r)^2}}{p} \quad (1)$$

where  $p$  is the pitch,  $\theta$  is the angle as shown in Fig. 2, and  $\ell_d$  is the actual length of the strand—the diagonal in Fig. 2.

This length increase directly corresponds to the increased dc resistance of a given strand. The overall dc resistance of a twisted bundle is the parallel combination of the resistances

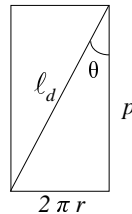


Fig. 2. The effect of twisting on the length of strand. See text.

of many such strands, each at a different radius. Because of the different resistance of stands at different radii, the dc current will not be exactly equal for each strand. However, the expression for total resistance is greatly simplified by assuming that the dc current flowing in each strand is the same. By performing both the simplified and exact calculations, we found that the approximation of equal dc strand currents is good to better than 2% when the pitch is more than six times the diameter of the bundle. Thus, we chose to use that simplified calculation for further analysis. Because the strand length depends on radius, the overall diameter or radius of the bundle must be known in order to calculate the dc resistance. The overall bundle diameter  $d_b$  depends on the strand packing factor, which we define as

$$K_a = \frac{A_e}{A_b} \quad (2)$$

where  $A_b$  is the overall bundle area ( $\pi d_b^2/4$ ) and  $A_e$  is the sum of the cross sectional areas of all the strands, with each strand area taken perpendicular to the bundle, not perpendicular to the strand. Thus, the area of each strand is taken at a different angle,  $\theta$ , to the strand axis, resulting in a elliptical area, as shown in Fig. 3. We assume that packing factor  $K_a$  is constant independent of the pitch. However, the bundle diameter increases with smaller pitch, as can be seen in this expression, derived in Appendix I,

$$d_b = \sqrt{\frac{nd_s^2}{K_a} \left(1 + \frac{\pi^2 nd_s^2}{4K_a p^2}\right)} \quad (3)$$

where  $n$  is the number of strands and  $d_s$  is the diameter of each strand. Using (3), Appendix I derives the dc resistance, based on equal currents in each strand:

$$R_{dc} = \frac{4\rho_c \ell}{\pi n d_s^2} \left(1 + \frac{\pi^2 n d_s^2}{4K_a p^2}\right) \quad (4)$$

where  $\ell$  is the length of the bundle and  $\rho_c$  is the resistivity of copper. The factor  $\frac{4\rho_c \ell}{\pi n d_s^2}$  represents resistance without twisting, and the expression in the parentheses represents the effect of pitch.

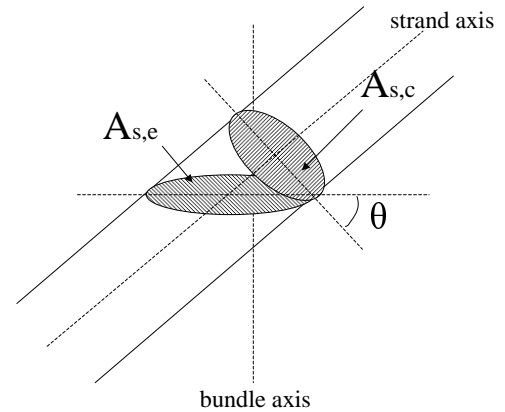


Fig. 3. In the cross section of the bundle the strand cross section becomes elliptical.

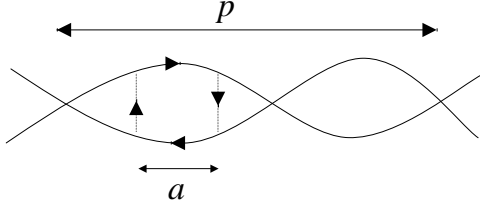


Fig. 4. Integration loop used to find voltage that induces current flow along the marked path.

### B. Strand-level eddy-current loss

For a single strand of length  $\ell_s$  placed in a sinusoidally varying magnetic field, the proximity-effect power loss can be modelled as [1], [3], [4], [5]

$$P_{pe} = \frac{\pi\omega^2 \hat{B}^2 d_s^4 \ell_s}{128\rho_c} \quad (5)$$

where  $\omega$  is the radian frequency and  $\hat{B}$  is the peak flux density, assumed to be constant throughout the strand. This assumption is equivalent to assuming the strand to be small compared to a skin depth at the frequency of interest [6]. In good designs, this will in fact be the case.

For the case of a transformer winding,  $\hat{B}$  varies with position. Thus in order to calculate the power loss for the whole winding, we use the spatial average of  $\hat{B}^2$ , which we write as  $\overline{\hat{B}^2}$ . The strand-level eddy-current loss for the whole transformer winding, taking into account of the effect of pitch as in the calculation of dc resistance, can be written as

$$P_{\text{eddy, strand}} = \frac{\pi\omega^2 \overline{\hat{B}^2} d_s^4 n \ell}{128\rho_c} \left(1 + \frac{\pi^2 n d_s^2}{4K_a p^2}\right) \quad (6)$$

In typical transformer designs, a standard one-dimensional model of the field is sufficient to obtain the average value of  $\hat{B}^2$  [7],

$$\overline{\hat{B}^2} = \frac{1}{3} \cdot \left(\frac{\mu_0 N \hat{I}}{b_w}\right)^2 \quad (7)$$

where  $b_w$  is the width of the winding window,  $N$  is the number of turns and  $\hat{I}$  is the peak current.

### C. Bundle-level eddy-current loss

In a twisted bundle with significant resistance between strands, the potential between a pair of strands can be calculated as the derivative of the integral of the flux linked by the path shown in Fig. 4. The area of the loop in Fig. 4 varies with the distance  $a$  between the positions where potential is evaluated. We assume that the flux is uniform throughout the bundle; that the eddy currents are not large enough to significantly reduce the flux. In Section V-A, we discuss the situation where eddy current is large enough to reduce the flux.

In a given cross section through the bundle, different strands are at different points in the twist cycle, corresponding to different values of  $a$ . Thus, if we describe the bundle cross section in polar coordinates  $(r, \phi)$ , the potential difference

between a strand and the strand in the corresponding position on the opposite side of the bundle depends on  $\phi$  (which determines  $a$ ), and on the radius  $r$ . Taking the center of the bundle as zero potential, we derive in Appendix II an expression for the potential at any point in a given cross section.

$$V(r, \phi) = \frac{rp}{2\pi} \sin(\phi) \omega \hat{B} \sin(\omega t) \quad (8)$$

This potential drives the currents between strands.

Instead of calculating interstrand currents for particular strands, we approximate the network of discrete resistances between strands as a continuous medium described by a resistivity  $\rho_{ss}$  in the plane perpendicular to the axis. Thus, we can calculate current and loss from the electric field which is found from the gradient of potential. The resulting time-average bundle-level proximity-effect loss is calculated in Appendix II to be

$$P_{\text{eddy, bundle}} = \frac{p^2 \omega^2 \overline{\hat{B}^2} n d_s^2 \ell}{32\rho_{ss} \pi K_a} \left(1 + \frac{n\pi^2 d_s^2}{4K_a p^2}\right). \quad (9)$$

Again, for typical transformer designs,  $\overline{\hat{B}^2}$  is given by (7), based on standard one-dimensional analysis [7].

We have now calculated all of the important losses in stranded wire. We see that interstrand resistivity,  $\rho_{ss}$ , and pitch,  $p$  are important parameters determining the amount of bundle-level proximity effect loss. Thus, we will address these two parameters in more detail in Sections III and IV.

## III. INTERSTRAND RESISTIVITY MEASUREMENTS

The resistivity of the bundle in the plane perpendicular to the axis,  $\rho_{ss}$ , is an important parameter in determining the bundle-level proximity-effect loss. If the resistance between strands is known, it is possible to calculate  $\rho_{ss}$ . Because we were unable to calculate all of the factors affecting resistance between strands, we used the apparatus shown in Fig. 5 to directly measure resistivity of a large number of strands packed into a rectangular region. When strands are bundled, the contact area increases with the increasing pressure packing the strands, and so the interstrand resistivity decreases with pressure. To enable quantifying this effect, the apparatus shown in Fig. 5 allows varying pressure through the force applied to a plunger. In order to measure only the resistance of contacts between strands, without measuring the contact resistance between the apparatus and the strands, interdigitated electrodes on top and bottom were used with a four-wire measurement technique.

We find that when strands are packed tightly (i.e., with high pressure, around 80 kPa) the interstrand resistivity ceases to change much with pressure. Thus, the resistivity at high pressure can be used for design without the need to determine the actual pressure in a given winding design.

Table I shows the experimental results at 80 kPa. There is no consistent pattern to the data; the results may be related more to the degree of oxidation or other contamination on the surface of the wire than to the diameter. Given the inconsistency of the data, it seems wise to design based on the worst-case lowest value of  $20 \mu\Omega\cdot\text{m}$ . However, even  $20 \mu\Omega\cdot\text{m}$  is over one thousand times higher than the resistivity of bulk copper. Thus, substantial

TABLE I  
INTERSTRAND RESISTIVITY UNDER 80 kPA PRESSURE

Wire size (AWG)	32	38	44
Bare copper wire	240 $\mu\Omega\cdot\text{m}$	75 $\mu\Omega\cdot\text{m}$	90 $\mu\Omega\cdot\text{m}$
Tinned copper wire	50 $\mu\Omega\cdot\text{m}$	20 $\mu\Omega\cdot\text{m}$	110 $\mu\Omega\cdot\text{m}$

decreases in loss can be expected even with no special efforts to increase resistivity. It is also possible to estimate interstrand resistivity from several different types of ac-loss measurements, as discussed in Section V.

#### IV. OPTIMAL PITCH

From (9), we see that the bundle-level eddy-current loss decreases as pitch is reduced. This is a direct result of the reduced size of the loop in Fig. 4. However, the other losses,  $P_r = I_{rms}^2 R_{dc}$  (where  $R_{dc}$  is given by (4)) and the strand-level eddy-current loss  $P_{eddy, strand}$  given by (6), increase as pitch is reduced. Thus, the total loss,  $P_{tot} = P_r + P_{eddy, strand} + P_{eddy, bundle}$ , can be expected to have a minimum value at an intermediate, optimal pitch,  $p_{opt}$ . This value can be found by setting the derivative of  $P_{tot}$  with respect to pitch equal to zero and solving for pitch.

$$p_{opt} = \sqrt[4]{\frac{\pi^4 \rho_{ss} n d_s^4}{16 \rho_c} + \frac{32 I_{rms}^2 \rho_{ss} \pi^2 \rho_c}{\omega^2 \hat{B}^2 n d_s^2}} \quad (10)$$

Because of bundle-level eddy-current loss, the optimal pitch is typically smaller than that found in standard commercial wire. However, there is no technical barrier to manufacturing wire with smaller pitches, now that there is an incentive to do so.

With an expression for the optimal pitch in-hand, the remaining choices are the number and diameter of strands. This design problem is then similar to the design problem for standard litz wire.

#### V. EXPERIMENTAL VERIFICATION OF LOSS PREDICTION

To verify the eddy-current loss predicted by (6) and (9), we constructed a 40-turn to 40-turn transformer on an ETD39

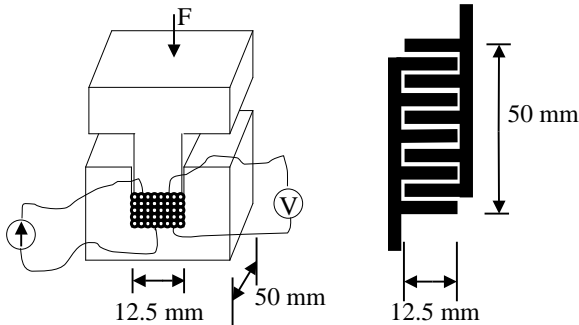


Fig. 5. Experimental apparatus for measuring the interstrand resistivity. Adjustable force can be applied such that the effect of pressure on the interstrand resistivity can be taken into account. The right side shows the interdigitated electrodes. These electrodes were placed on the top and bottom of the rectangular region where wires were packed. With these electrodes, contact resistance between electrodes and strands will not be included in the measurement.

size ferrite core. Both windings used wire with 66 uninsulated strands of 40 AWG (80  $\mu\text{m}$  diameter) tinned copper, twisted with a pitch  $p = 8$  mm. The overall bundle is insulated with a thermoplastic coating. To reduce capacitance and dielectric losses, and to facilitate high-frequency measurements, thick polypropylene tape was used between winding layers. Measurements were performed with the two windings connected in series opposition, to ensure perfectly balanced leakage excitation [8]. With the polypropylene tape, the self-resonant frequency in this configuration was 15.8 MHz, well above the frequency range of 1 kHz to 500 kHz that we measured.

Fig. 6 shows the measured ac resistance factor, along with two theoretical curves based on our model with different values of interstrand resistivity  $\rho_{ss}$ : the worst-case value of 20  $\mu\Omega\cdot\text{m}$  and the value that gives the best fit to the measured data in the low-frequency region, 25  $\mu\Omega\cdot\text{m}$ . We chose a value to fit the measurements in the low-frequency region because the deviation in the high-frequency region is likely due to self-shielding of the bundle. We will discuss the self-shielding effect in more detail in section V-A.

Also in Fig. 6 is the measured ac resistance factor of a single-strand 22 AWG (0.64 mm diameter) winding. The diameter of the single strand is slightly smaller than the overall stranded bundle (0.7 mm diameter), but it still has about 10% lower dc resistance. Considering dc resistance and ac resistance factor, the net ac resistance of the two designs is equal at 15 kHz; above this frequency the performance of the stranded-wire winding is superior, typically by a large margin. Note that this is without using the optimal pitch, as calculated in Section IV. At 100 kHz, for example, the optimal pitch would be 4.6 mm instead of the actual 8 mm, and would decrease the overall loss by 8%; at 300 kHz, the optimal pitch is 2.9 mm, and is calculated to reduce the overall loss by 43%.

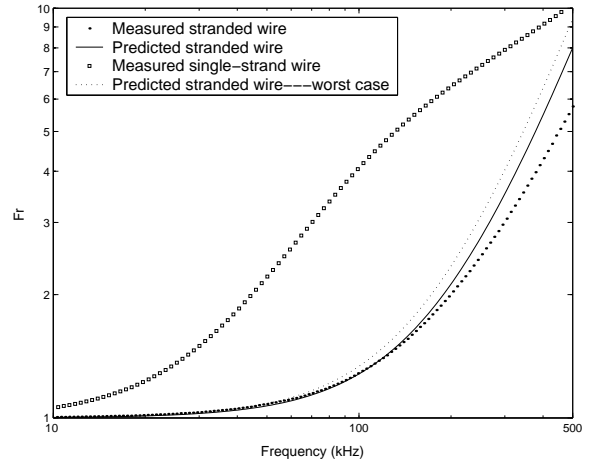


Fig. 6. Experimental ac resistance factor  $F_r = R_{ac}/R_{dc}$  for a transformer wound with stranded wire with 66 uninsulated 40 AWG strands, or with 22 AWG solid wire. Compared with a solid-wire winding, a stranded-wire winding provides a great loss reduction. Our model predicts the loss in stranded wire with high accuracy up to 100 kHz and reduced accuracy up to 500 kHz.

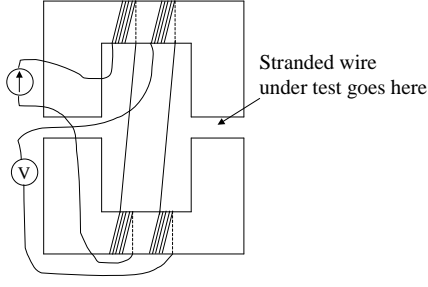


Fig. 7. Experimental apparatus used to measure proximity effect eddy-current loss in stranded wire. Two windings are used, as in a standard core-loss measurement, such that the measurement (performed with an impedance analyzer) does not include loss in these windings. However, the measurement does include eddy-current loss induced in a wire sample placed in the gap. The windings have a total of ten turns each, five on each core-half (Ferroxcube U93/76/30 size of 3C85 ferrite).

### A. Self-shielding effect

The bundle-level self-shielding effect occurs when the magnetic field generated by the bundle-level eddy current is large enough to reduce the original magnetic field which induces the eddy current. Thus the magnetic field in the center of the bundle is reduced. As defined and calculated in Appendix III, the onset frequency of the self-shielding effect is

$$f_{onset} = \frac{4\pi\rho_{ss}}{\mu_0 p^2} \quad (11)$$

To look at the self-shielding effect in more detail, we set up a measurement apparatus as shown in Fig. 7 to directly measure proximity-effect loss. With this apparatus we use four terminal impedance measurement to detect losses in this gapped transformer. When there is no wire in the gap, it detects the core loss; when we put wire in the air gap, eddy current loss is induced in the wire and this loss will simply add to the measured loss. To determine the loss in the wire, we subtract the core loss from the total loss.

Suppose there is a sinusoidal current with rms amplitude  $I$  flowing in the primary winding. With the secondary winding open, the flux density in the air gap is

$$\hat{B} = \frac{\mu_0 N \sqrt{2} I}{2\ell_g} \quad (12)$$

where  $\ell_g$  is the length of air gap. Thus the power loss in the wire will be

$$P_{wire} = \left(1 + \frac{\pi^2 n d_s^2}{4K_a p^2}\right) \left(\frac{\pi \omega^2 \hat{B}^2 d_s^4 n \ell}{128 \rho_c} + \frac{p^2 \omega^2 \hat{B}^2 n d_s^2 \ell}{32 \rho_{ss} \pi K_a}\right) \quad (13)$$

Substituting (12) into (13) and dividing both sides of (13) by  $I^2$  yields

$$R_{pe} = \left(1 + \frac{\pi^2 n d_s^2}{4K_a p^2}\right) \left(\frac{\pi \omega^2 d_s^4 n \ell}{128 \rho_c} + \frac{p^2 \omega^2 n d_s^2 \ell}{32 \rho_{ss} \pi K_a}\right) \left(\frac{\mu_0^2 N^2}{2\ell_g^2}\right). \quad (14)$$

where  $R_{pe}$  is the measured increase in the real part of impedance when the wire is inserted into the gap. Thus in the measurement, we do not need to know the current flowing in the primary winding.

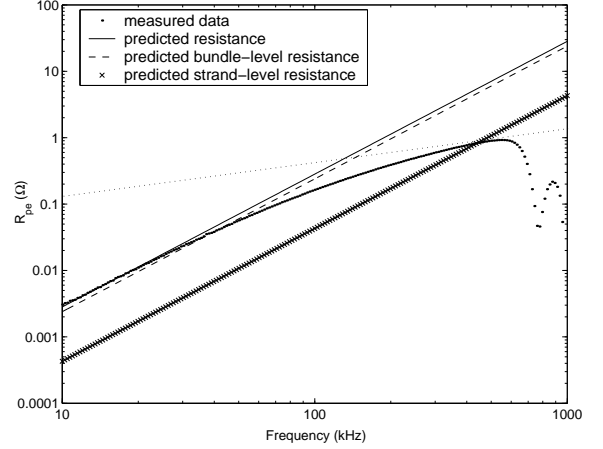


Fig. 8. Measurement of proximity-effect loss in wire with 65 strands of AWG 30 tinned copper wire, using the apparatus in Fig. 7. The vertical axis ( $R_{pe}$ ) is the measured increase in the real part of impedance when the wire is inserted into the gap. The decreased slope of the measured loss at high frequencies is believed to be due to the self-shielding effect of bundle-level eddy currents. The calculated onset frequency of this effect is 237 kHz. To estimate the experimental onset frequency, the dotted line with slope 0.5 is drawn tangent to the measured data. It crosses the low-frequency asymptote at about 130 kHz, indicating a lower onset frequency than calculated, but it is difficult to determine this accurately because the accuracy of the measurement is degraded at high frequencies by a resonance in the apparatus around 800 kHz. Parameters for the stranded wire tested are  $p = 32.5$  mm,  $\rho_{ss} = 25 \mu\Omega\cdot\text{m}$ ,  $\ell = 100$  mm.

Two wire samples were measured and the data are shown in Fig. 8 and Fig. 9.

In both figures, the predicted resistance is plotted along with bundle-level and strand-level resistances. For each wire sample, a interstrand resistivity,  $\rho_{ss}$ , is chosen to fit the measured data. Using (11), we calculate the onset frequencies of the self-shielding effect to be 237 kHz and 625 kHz for the two samples.

We wish to compare the experimental result with this calculation. However, it is difficult to clearly identify the onset frequency in the experimental data. We expect that, as in solid wire, the ac resistance will be proportional to the square root of frequency in the high-frequency region well above the onset of self-shielding. In Figs. 8 and 9 this high-frequency asymptote is represented by a dotted line with a slope of 0.5, chosen to be tangent to the measured curve. The intersection with the low-frequency predicted resistance line then defines the measured onset frequency. Unfortunately, the resonant frequency of the apparatus occurs near the onset frequency, at about 800 kHz. Thus, the data does not include a large enough portion with slope of 0.5 to allow an accurate determination of this asymptote, and our experimental measurements are only rough estimates of the onset frequency. This difficulty is particularly severe in Fig. 9 which has the higher onset frequency.

Despite these limitations, the experiment is a useful confirmation of the trends in onset frequency, and it confirms the predicted order of magnitude of the frequency at which the self-shielding effect becomes significant: For the wire with 65 strands, the measured onset frequency (as we have defined it graphically) is about 130 kHz, while for the wire with 41 strands, it is about 300 kHz. Both measurements are about a factor of two below the calculated onset frequencies.

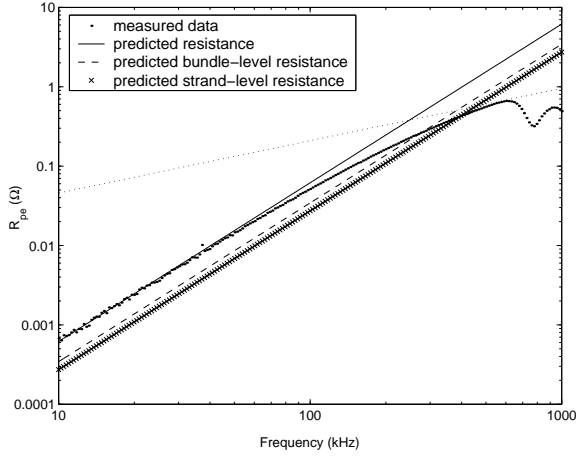


Fig. 9. Measurement of proximity-effect loss in wire, similar to Fig. 8, but with 41 strands of AWG 30 tinned copper wire. Again, the decreased slope of the measured loss at high frequencies is believed to be due to the self-shielding effect of bundle-level eddy currents. The calculated onset frequency of this effect is 625 kHz, and the estimated experimental onset frequency is about 300 kHz. However, it is very difficult to determine this point accurately because of its proximity to the 800 kHz resonance of the apparatus. Parameters for the stranded wire tested are  $p = 20$  mm,  $\rho_{ss} = 25 \mu\Omega\cdot\text{m}$ ,  $\ell = 100$  mm.

## VI. CONCLUSION

Stranded wire can be a useful low-cost alternative to high-cost litz wire. Both the cost of insulating individual strands, and the cost of terminating the litz wire can be avoided or decreased.

In order to make the use of stranded wire a viable alternative, it is necessary to be able to predict high-frequency losses in it. These losses include the same strand-level eddy-current and resistive losses as in litz wire, plus bundle-level eddy-current effects arising from the finite interstrand resistivity. We have presented an analysis of this loss, plus improvements to models of strand-level eddy-current and resistive losses to precisely account for the effect of pitch.

Important parameters in determining the performance of stranded wire are the resistance between strands and the pitch. Interstrand resistivity has been characterized, and a worst-case value proposed for use in design. An optimal pitch has been found for minimum total loss.

Experimental measurements verify the model and show dramatic advantages over the performance of a solid-wire winding without the high cost of litz wire. Discrepancies between prediction and measurement at very high frequency due to the bundle self-shielding effect have been discussed. Above the self-shielding onset frequency where the loss calculation is not accurate, it over estimates actual losses such that designs based on our model will be conservative. With the models and data we provide, designers can now take advantage of this opportunity for large savings in cost and loss.

## APPENDIX I CALCULATION OF DC RESISTANCE

The diameter of the bundle will increase with twisting. As defined in (2),  $K_a$  is the packing factor and is assumed to be

constant independent of pitch. Now we consider the situation when a bundle of  $n$  strands is twisted. In the bundle cross section, each strand area is elliptical, at an angle,  $\theta$ , to the strand, shown in Fig. 3. Note that at different radii,  $\theta$  has different values. From the elliptical area, we can calculate cross sectional area perpendicular to the strand.

$$A_{s,c} = A_{s,e} \cos(\theta) \quad (15)$$

where  $A_{s,c}$  is the cross sectional area of the strand perpendicular to the strand and  $A_{s,e}$  is the cross sectional area of the strand perpendicular to the bundle. As  $K_a$  is independent of pitch,

$$K_a = \frac{nA_{s,c}}{A_{b,0}} \quad (16)$$

where  $A_{b,0}$  is the overall bundle area when there is no twisting. The total cross sectional area of copper perpendicular to each strand is

$$A_c = nA_{s,c} = K_a A_{b,0} = K_a \frac{\pi d_0^2}{4} \quad (17)$$

where  $d_0$  is the bundle diameter without twisting. In a twisted bundle,  $A_c$  can be calculated as

$$A_c = \sum_{i=1}^n A_{s,e,i} \cos(\theta_i) \quad (18)$$

And this can be approximated as

$$A_c = \int_0^{\frac{d_b}{2}} K_a \cos(\theta) 2\pi r dr \quad (19)$$

Combining (17) and (19), we get the bundle diameter with twisting.

$$d_b = d_0 \sqrt{1 + \frac{\pi^2 n d_s^2}{4 K_a p^2}} \quad (20)$$

Substituting in  $d_0$

$$d_0 = \sqrt{\frac{n d_s^2}{K_a}} \quad (21)$$

results in the equation for bundle diameter (3).

The DC power loss of a single strand is

$$P_{dc,s} = I_s^2 \rho_c \frac{\ell d}{\frac{1}{4} \pi d_s^2} \quad (22)$$

where  $I_s$  is the rms current in each strand. In the cross section of a twisted bundle, DC power loss per unit area is

$$P_{dc,unit} = \frac{P_{dc,s}}{\frac{A_{s,e}}{K_a}} = \frac{16 K_a I_s^2 \rho_c \ell}{\pi^2 d_s^4} \quad (23)$$

We integrate over the bundle to get the total DC power loss

$$P_{dc} = \int_0^{\frac{d_b}{2}} P_{dc,unit} 2\pi r dr = P_{dc,0} \left(1 + \frac{\pi^2 n d_s^2}{4 K_a p^2}\right) \quad (24)$$

where  $P_{dc,0}$  is DC loss of the bundle without twisting. Now it is easy to calculate the DC resistance of the twisted bundle

$$R_{dc} = \frac{4 \rho_c \ell}{\pi n d_s^2} \left(1 + \frac{\pi^2 n d_s^2}{4 K_a p^2}\right) \quad (25)$$

where  $\frac{4 \rho_c \ell}{\pi n d_s^2}$  represents resistance without twisting.

## APPENDIX II

### CALCULATION OF BUNDLE-LEVEL EDDY-CURRENT LOSS

Fig. 10 shows the integration loop (marked with arrows) used to find voltage that induces current flow between strands, as in Fig. 4, but with coordinates. The area of the loop in Fig. 10 varies with distance  $a$  between the positions where potential is evaluated.

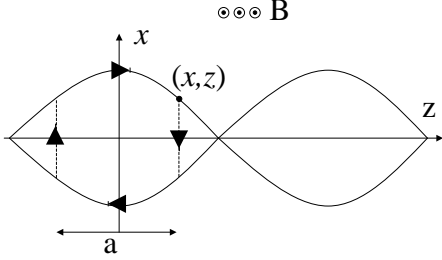


Fig. 10. Integration loop used to find voltage that induces current flow along the marked path.

The coordinates of the marked point on the loop  $(x, z)$  can be expressed as

$$x = r \cos(\phi) \quad z = \frac{p}{2\pi} \phi \quad (26)$$

Then the area of the loop projected on the  $xz$  plane is

$$A_{loop} = 4 \int_0^{\frac{a}{2}} x dz = \frac{2rp}{\pi} \sin\left(\frac{\pi a}{p}\right) \quad (27)$$

Thus, if we describe the bundle cross section in polar coordinates  $(r, \phi)$ , the potential difference between a strand and the strand in the corresponding position on the opposite side of the bundle depends on  $\phi$  (which determines  $a$ ), and on the radius  $r$ . The time varying flux density is

$$B = \hat{B} \cos(\omega t) \quad (28)$$

According to Faraday's Law, the potential can be found from the derivative of flux with respect to time. Taking the center of the bundle as zero potential, the potential at the point  $(r, \phi)$  is

$$V(r, \phi) = -\frac{d(\frac{1}{4}BA)}{dt} = \frac{rp}{2\pi} \sin(\phi) \omega \hat{B} \sin(\omega t) \quad (29)$$

The electric field can be found from the gradient of potential.

$$E(r, \phi) = -\nabla V = -\frac{p}{2\pi} \omega \hat{B} \sin(\omega t) [\hat{r} \sin \phi + \hat{\phi} \cos \phi] \quad (30)$$

Instead of calculating interstrand currents for particular strands, we approximate the network of discrete resistances between strands as a continuous medium described by a resistivity  $\rho_{ss}$  in the plane perpendicular to the axis. Thus we calculate the loss from the electric field

$$P(t) = \int_v \frac{E^2}{\rho_{ss}} dv = \frac{p^2 \omega^2 \hat{B}^2 n d_s^2 \ell}{16 \rho_{ss} \pi K_a} \left(1 + \frac{n \pi^2 d_s^2}{4 K_a p^2}\right) \sin^2 \omega t \quad (31)$$

Taking the time-average of (31) and using (7), results in an expression for bundle-level proximity-effect loss (9).

## APPENDIX III

### CALCULATION OF SELF-SHIELDING EFFECT ONSET FREQUENCY

The self-shielding effect occurs when the magnetic field generated by the eddy current is large enough to reduce the original magnetic field which induces the eddy current. The full calculation of the field as a combination of applied field and eddy field is complicated. To make the calculation simpler, we assume that the eddy current is only due to the applied field and is not affected by eddy current. Thus we define the onset frequency as the frequency at which the field due to eddy current in the center of the bundle matches the applied field.

Having the electric field in a given bundle cross section (30), we can calculate the volume current density.

$$J_v(r, \phi) = \frac{E(r, \phi)}{\rho_{ss}} \quad (32)$$

And the surface current density at a specific angle is

$$J_s(\phi) = \frac{J_v r_b \cos(\phi)}{\sin(\theta)} \quad (33)$$

Only the axial component of the surface current will contribute to eddy field to reduce the applied field.

$$J_{s,z}(\phi) = J_s(\phi) \cos(\theta) \quad (34)$$

Now we can integrate over the circle to get the flux density due to eddy current in the center of the bundle.

$$B_{center} = \int_0^{2\pi} \frac{\mu_0 J_{s,z}(\phi)}{2\pi} \cos(\phi) d\phi = \frac{\mu_0 p \omega r_b \cot(\theta)}{4\pi \rho_{ss}} \hat{B} \sin(\omega t) \quad (35)$$

Setting the magnitude of this flux density equal to the magnitude of applied flux density, we get the onset frequency of the self-shielding effect.

$$f_{onset} = \frac{4\pi \rho_{ss}}{\mu_0 p^2} \quad (36)$$

## REFERENCES

- [1] P. N. Murgatroyd, "Calculation of proximity losses in multistranded conductor bunches", *IEE Proceedings, Part A*, vol. 36, no. 3, pp. 115–120, 1989.
- [2] J. A. Ferreira, "Analytical computation of ac resistance of round and rectangular litz wire windings", *IEE Proceedings-B Electric Power Applications*, vol. 139, no. 1, pp. 21–25, Jan. 1992.
- [3] B. B. Austin, "The effective resistance of inductance coils at radio frequency", *The Wireless Engineer*, vol. 11, pp. 12–16, Jan. 1934, Summary of work by S. Butterworth.
- [4] C. R. Sullivan, "Optimal choice for number of strands in a litz-wire transformer winding", *IEEE Transactions on Power Electronics*, vol. 14, no. 2, pp. 283–291, 1999.
- [5] E. C. Snelling, *Soft Ferrites, Properties and Applications*, Butterworths, second edition, 1988.
- [6] Xi Nan and C. R. Sullivan, "An improved calculation of proximity-effect loss in high-frequency windings of round conductors", *34th Annual IEEE Power Electronics Specialists Conference*, 2003.
- [7] R. W. Erickson and D. Maksimovic, *Fundamentals of Power Electronics*, Kluwer Academic Publishers, second edition, 2001.
- [8] J. G. Hayes, N. O'Donovan, M.G. Egan, and T. O'Donnell, "Inductance characterization of high-leakage transformers", *Eighteenth Annual IEEE*, vol. 2, pp. 1150–1156, 2003.